JOURNAL OF MATERIALS SCIENCE **36** (2001) 3385–3394

Multiple grain growth events in liquid phase sintering

PEIZHEN LU, R. M. GERMAN
P/M Lab, 147 Research West, The Pennsylvania State University, University Park, PA 16802-6809, USA
E-mail: rmg4@psu.edu

Sintered tungsten heavy alloys consist of a solidified liquid alloy matrix phase which interpenetrates a solid tungsten skeletal structure. A consequence of liquid phase sintering is considerable grain growth while the compact densifies. The driving force for grain growth is a decrease in the interfacial surface energy, and the process itself is the combined result of liquid diffusion, solid diffusion, and vapor diffusion if porosity is present. In this study, we utilized microgravity sintered samples to avoid solid-liquid segregation to study the multiple diffusion processes. Coupled with the diffusion event through the liquid phase, there is simultaneous solid-state sintering such as coalescence. The dihedral angle determines the contiguity and the grain growth rate. The liquid diffusion grain growth rate constant is at least one order of magnitude larger than the solid diffusion grain growth rate constant. As composition changes, the ratio of grain growth contributions from these three components also changes, which, in turn, causes grain size, grain size distribution, and contiguity variations.

1. Introduction

In the most general term, all sintering processes can be considered as liquid phase sintering, with solid-state sintering treated as the limiting situation where the liquid volume equals zero. During the initial stage of the sintering cycle, the microstructure consists of solid grains and porosity. Solid bonds form as temperature activates diffusion processes. After liquid formation at higher temperatures, the liquid provides both a capillary force and a transport medium to promote densification [1]. Depending on the solid skeleton formation and the amount of liquid available, porosity will be eliminated at a rate dependent on the capillary force and the compact rigidity. After sintering, the microstructure is characterized by grains of the higher melting phase exhibiting a rounded shape and filling the space effectively in a matrix of liquid phase with or without residual porosity. Often this microstructural development is accompanied by a pronounced growth of the solid grains and a marked reduction or even elimination of porosity.

The classic expression for grain growth via Ostwald ripening derived by Lifshitz and Slyzonov [2] and Wagner [3] is valid only when there is no grain-grain contact. For tungsten heavy alloys, the solid content must be high for compact shape retention. In such a solid-liquid system, the solid skeletal structure forms during heating, thereby altering the coarsening process. To accommodate the presence of solid phase connectivity, it is essential to take into account the interactions between the diffusion fields around the grains. Modifications [4] have been proposed to account for grain growth via coalescence associated with high solid volume fractions. This includes solid diffusion grain growth and the pore pinning effect on grain growth. Based on this, knowing different diffusion mechanism contributions to microstructural development is essential in providing information on (1) how microstructure evolves during sintering, (2) what forces and material transport processes are active during sintering, and (3) how the resulting microstructure is related to the processing conditions and compositions.

When liquid phase sintering is carried out under gravity, solid-liquid segregation occurs because there are few systems where the solid and liquid densities are equal. Furthermore, porosity varies with position due to a strong buoyancy force. A system with a higher density difference between the solid and liquid phases will attempt to settle the solid grains at the sample bottom (assuming a higher solid density) during liquid phase sintering due to pronounced settling forces. This problem is especially true when the solid and liquid phase densities are very different, such as tungsten heavy alloys. Liu *et al*. [5] developed a model to predict the slumping of materials with high solid-liquid differences; the three-dimensional packing coordination number at sample height H is:

$$N_C(H) = N_{C0} + KA(H) \tag{1}$$

with N_{C0} as a constant, K as the compression factor, and $A(H)$ as the accumulated volume fraction of the solid above the position H.

Besides slumping, solid-liquid segregation, and grain packing, sintering kinetics and grain growth can also exhibit changes with gravity-induced structural variations

[6–10]. If the liquid content is high, solid grain growth is faster at the sample bottom than near the top. The effect of gravity is larger in the specimens with a lower dihedral angle. Likewise, pores experience buoyancy forces that cause accumulation near the compact top and migrate to the liquid phase where they can be eliminated in the first several minutes after liquid formation.

Seyhan *et al*. [11] presented a study on the dispersion of lead particles in a near-eutectic Pb-Sn liquid which was stabilized against gravitationally induced sedimentation by the use of Lorentz forces. The results show that solid volume fraction has a definite effect on the rate of grain coarsening. However, the study cannot produce conclusive results on the multiple diffusion mechanisms in liquid phase sintering since Lorentz forces accelerate the coarsening process when a solid skeleton is present. Up to now, no connection is established for the simultaneous solid, liquid, and pore phase effect on grain growth. Understanding of this three-phase problem is fundamental to liquid phase sintering since the majority of grain growth occurs during initial densification.

Microgravity liquid phase sintering provided a means to research macroscopic and microstructural changes without the complications from buoyancy forces [12–14]. The effect of gravity on sintering shrinkage and dimensional uniformity were analyzed using a continuum theory of sintering [15, 16]. An algorithm was introduced for minimization of gravity-induced shrinkage anisotropy, suggesting an asymptotic approach to the peak temperature for best dimensional uniformity. The studies also showed that shape distortion accumulated during solid-state sintering should be taken into account when considering gravity effects. On the microscopic scale, grain agglomeration and segregation were observed in solid-liquid mixtures sintered under microgravity conditions [7]. German *et al*. [6] compared grain sizes of tungsten heavy alloys sintered on Earth and under microgravity conditions; the microgravity samples consistently produced a smaller grain size. In this study, we utilize this advantage to 'suspend' tungsten grains in the liquid phase to study multiple diffusion mechanisms during sintering. The approach is ideal to separate different grain growth events and find their relationship with the system composition and processing conditions.

2. Analysis

Solid, liquid, and pores usually coexist in liquid phase sintering as evident in Fig. 1. A certain degree of solid-solid contact occurs in liquid phase sintering depending on solid content, grain shape, and surface energy. As German and Olevsky [4] pointed out, several mechanisms are potentially active contributors to grain growth, including solution-reprecipitation, solid-state coalescence, and vapor diffusion. To correctly describe the grain growth process in liquid phase sintering, liquid, solid, and possible vapor transport paths should be considered. Instantaneous grain growth in liquid phase sintering is determined by the sum of the individual contributing events:

$$\frac{\mathrm{d}V}{\mathrm{d}t} = \sum_{i=1}^{N} X_i \frac{\mathrm{d}V_i}{\mathrm{d}t} \tag{2}$$

$\frac{\mathrm{d}V}{\mathrm{d}t}$: the total volumetric rate of grain growth for a grain with volume V at sintering time t, X_i: the weight

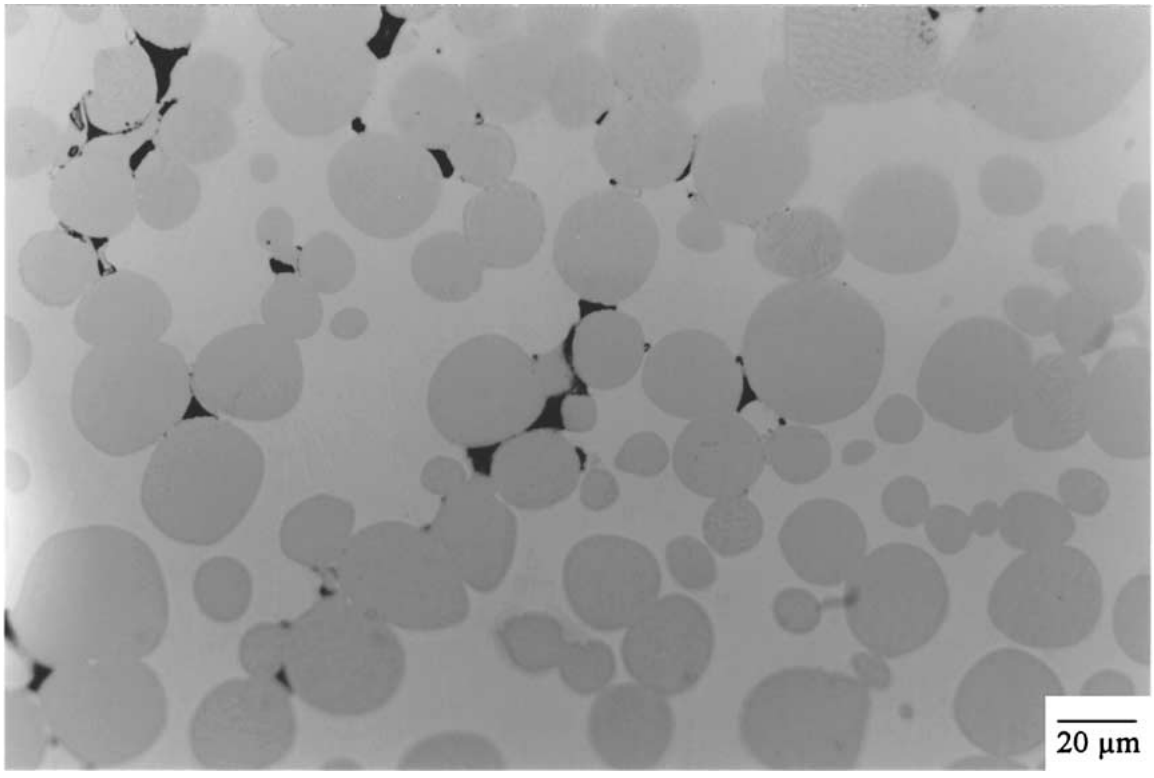

Figure 1 Optical micrograph showing the coexistence of solid (circular phase), liquid (light color phase), and pores (dark color phase) in a 88W-Ni-Cu (Ni : Cu = 8 : 2) sample after 1500°C, 1 min microgravity sintering.

coefficient of grain growth mechanism i, N: total number of grain growth mechanisms, $\frac{dV_i}{dt}$: the volumetric rate of grain growth for a grain through mechanism i.

Conceptually, we can expect the weight coefficient X_i is a function of microstructure, where solid diffusion grain growth is dominant at high solid contents and liquid processes are dominant at high liquid contents. Porosity shields atomic transport through solid or liquid diffusion by reducing the effective diffusion area. Hence, as a first guess:

$$X_{\mathrm{i}} = \frac{K_{\mathrm{i}} \cdot S_{\mathrm{Si}}}{K} = \frac{K_{\mathrm{i}} \cdot S_{\mathrm{Si}}}{\sum_{i=1}^{N} K_{\mathrm{i}} \cdot S_{\mathrm{Si}}} \tag{3}$$

K: overall grain growth rate constant, K_i: grain growth rate constant for mechanism i, S_{Si}: interfacial area fraction between solid grain and phase i.

Since there are only liquid, solid, and vapor phases around a grain, more directly:

$$K = K_{\mathrm{L}} \cdot S_{\mathrm{SL}} + K_{\mathrm{S}} \cdot S_{\mathrm{SS}} + K_{\mathrm{V}} \cdot S_{\mathrm{SV}} \tag{4}$$

The overall grain growth rate constant K will depend on the flux of atoms through solid, liquid, and vapor phases.

If the grain size is G, then the grain volume V and surface area S are, respectively:

$$V = g_{\mathrm{V}} G^3 \tag{5}$$

$$S = g_{\mathrm{S}} G^2 \tag{6}$$

g_{v}, g_{s}: geometry factors

From Equation (2):

$$\frac{\mathrm{d}G^3}{\mathrm{d}t} = \frac{1}{g_{\mathrm{V}}}\left(\left.\frac{\mathrm{d}G^3}{\mathrm{d}t}\right|_{\mathrm{L}} + \left.\frac{\mathrm{d}G^3}{\mathrm{d}t}\right|_{\mathrm{V}} + \left.\frac{\mathrm{d}G^3}{\mathrm{d}t}\right|_{\mathrm{S}} \right) \tag{7}$$

subscript L, V, and S represent the contribution from liquid, vapor, and solid diffusion mechanisms.

For liquid and vapor diffusions, Fick's first law can be applied:

$$J = \sum_{i=1}^{N} J_i = -\sum_{i=1}^{N} D_i \frac{\partial C_i}{\partial x} \tag{8}$$

J: total flux, J_i: flux through phase i, D_i: diffusivity through phase i, $\frac{\partial C_i}{\partial x}$: concentration gradient when atom diffuses to solid grain through phase i.

Since the total flux J is the amount of atoms passing through unit area in unit time, from Equations 2 and 5:

$$\frac{\mathrm{d}V}{\mathrm{d}t} = J \cdot S \cdot \Omega = -\Omega \sum_{i=1}^{N} D_i \frac{\partial C_i}{\partial x} S_i \tag{9}$$

Ω: molar volume of the diffusing species, S: total grain surface area, S_i: grain surface area experiencing diffusion mechanism i

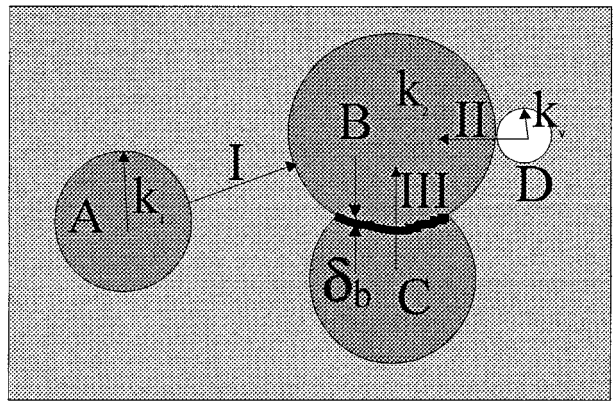

Figure 2 Configuration showing possible diffusion mechanisms in solid-liquid-pore coexisting system. I: liquid diffusion, II: vapor diffusion, III: solid diffusion. k_1, k_2, and k_{V} respectively represents the curvature of shrinking grain A, growing grain B, and pore D. Grain C represents the shrinking grain undergoing solid diffusion. δ_{b} is the grain boundary thickness.

$$\left.\frac{\mathrm{d}G^3}{\mathrm{d}t}\right|_{L} + \left.\frac{\mathrm{d}G^3}{\mathrm{d}t}\right|_{V} = -\frac{1}{g_V}\Omega\left(D_{\mathrm{L}} \frac{\partial C_L}{\partial x} S_{\mathrm{SL}} g_{\mathrm{S}} G^2 + D_{\mathrm{V}} \frac{\partial C_{\mathrm{V}}}{\partial x} S_{\mathrm{SV}} g_{\mathrm{S}} G^2 \right) \tag{10}$$

To obtain diffusing species concentration gradient, the curvature at a certain grain surface location should be considered. Fig. 2 suggests how these different mechanisms can be combined. For liquid diffusion (path I):

$$\frac{\partial C_{\mathrm{L}}}{\partial x} = \frac{C_{\mathrm{L}O}\,\Omega \gamma_{\mathrm{SL}}}{kT d_{\mathrm{L}}}(k_1 - k_2) \tag{11}$$

C_{LO}: diffusing species equilibrium concentration in the liquid phase, γ_{SL}: solid-liquid interfacial energy, k: Boltzmann constant, T: absolute temperature, k_1: grain A surface curvature, k_2: grain B surface curvature, d_{L}: diffusion distance in the liquid phase.

Since d_{L}, k_1, and k_2 are all functions of grain size G, there exists a function A_{L}:

$$\frac{A_{\mathrm{L}}}{G^2} = \frac{1}{d_{\mathrm{L}}}(k_1 - k_2) \tag{12}$$

Substitute (12) into (11):

$$\frac{\partial C_{\mathrm{L}}}{\partial x} = \frac{C_{\mathrm{L}O} A_{\mathrm{L}} \Omega \gamma_{\mathrm{SL}}}{kT G^2} \tag{13}$$

For vapor diffusion (path II):

$$\frac{\partial C_{\mathrm{V}}}{\partial x} = \frac{C_{\mathrm{V}O}\,\Omega \gamma_{\mathrm{SV}}}{kT d_{\mathrm{V}}}(k_{\mathrm{V}} - k_1) \tag{14}$$

$C_{\mathrm{V}O}$: diffusing species equilibrium concentration in the vapor phase, γ_{SV}: solid-vapor interfacial energy, k_V: pore D surface curvature, d_V: diffusion distance in the vapor phase.

By the same means as in the liquid phase, there exists a function A_V:

$$\frac{A_V}{G^2} = \frac{1}{d_V}(k_V - k_2) \tag{15}$$

Substitute (15) into (14):

$$\frac{\partial C_V}{\partial x} = \frac{C_{VO} A_V \Omega \gamma_{SV}}{kT G^2} \tag{16}$$

For solid-state diffusion (path III), the intrinsic motion of the grain boundary from the expanding grain B to the shrinking grain C is determined by the diffusional transfer of matter from the grain C to the grain B. The mobility of an atom crossing the boundary, M, is given as:

$$M = \frac{D_S}{kT} \tag{17}$$

The average driving force for grain boundary motion F_b [17, 18]:

$$F_b = \frac{c\gamma_{SS}\Omega}{\delta_b G} \tag{18}$$

c: constant, γ_{SS}: grain boundary energy, δ_b: grain boundary thickness.

The average rate of grain growth by solid diffusion, $\frac{dG}{dt}|_s$, is related directly to the average velocity, v_b, of the migrating boundaries through:

$$\left.\frac{dG}{dt}\right|_s = 2v_b S_{SS} = 2MF_b S_{SS} = \frac{2c\gamma_{SS}\Omega D_S S_{SS}}{\delta_b G k T} \tag{19}$$

subscript S indicates the contribution from solid diffusion.

Combine (7), (10), (13), (16), and (19):

$$\begin{aligned}\frac{dG}{dt} &= \left.\frac{dG}{dt}\right|_L + \left.\frac{dG}{dt}\right|_V + \left.\frac{dG}{dt}\right|_S \\ &= \frac{K_S S_{SS}}{G} - \frac{K_L S_{SL} + K_V S_{SV}}{G^2}\end{aligned} \tag{20}$$

where:

$$K_L = \frac{C_{LO} D_L \gamma_{SL} A_L g_S \Omega^2}{3 g_V k T} \tag{21}$$

$$K_V = \frac{C_{VO} D_V \gamma_{SV} A_V g_S \Omega^2}{3 g_V k T} \tag{22}$$

$$K_S = \frac{2c\gamma_{SS}\Omega D_S}{\delta_b k T} \tag{23}$$

Indeed, the model is applicable to any multiple phase microstructure where concurrent, independent transport paths contribute to grain growth.

When the porosity in the sample is zero:

$$\frac{dG}{dt} = \frac{K_S S_{SS}}{G} - \frac{K_L S_{SL}}{G^2} \tag{24}$$

When $K_L S_{SL} = R$, $K_S S_{SS} = \frac{R}{G^*}$, Equation 24 is Greenwood's Equation [19], which only considers grain growth for a dilute suspension. R is a combination of features that include diffusivity, surface energy, solubility, and atomic volume; G^* is the critical grain size.

3. Experimental procedures

In this experiment, the heavy alloy composition is 88W-Ni-Cu (Ni : Cu = 8 : 2 or 6 : 4) in weight percent. The W-Ni-Cu system was chosen because of the extremes in the solubility behavior of tungsten in the respective matrix components. Copper has practically no solubility for tungsten. Nickel, on the other hand, dissolves tungsten up to a maximum of 17 wt% while decreasing the solid-liquid surface energy. Even a small amount of nickel has a dramatic effect on both parameters. The characteristics of the tungsten, nickel, and copper powders are given in Table I. The mixed powders were cold isostatically pressed at 210 MPa and presintered in hydrogen at 1000°C for 1 h to increase the compact strength. Each of the samples was 8.2 mm in diameter and height after presintering. Four sintering times were chosen for microgravitational sintering at 1500°C: 1, 45, 180, and 600 min. During sample preparation for the flight, each sample was placed in its own alumina crucible. The loaded crucibles were stacked such that the bottom of one crucible became the top of the one beneath it. The stack of crucibles was then placed in a boron nitride container, which was then sealed in tantalum containment cylinders. At each stage, the appropriate outermost container was evacuated to prevent expansion of entrapped gas and possible rupture of the cartridge. The cartridges were then directly loaded into the Large Isothermal Furnace (LIF) as part of the Microgravity Science Laboratory mission (MSL-1) aboard the Space Shuttle *Columbia* in 1997. The heating rate was 18°C/min and the cooling rate was 3°C/min. The peak acceleration during sintering was 3.0×10^{-4} g with an average value of 2.12×10^{-6}g.

After completion of the sintering experiments and return of the cartridges to Earth, the sample density was measured through Archimedes method before longitudinally sectioning and metallographically polishing. The samples were observed using an optical microscope. The images were digitally processed and quantified. The quantification procedure was as follows: the

TABLE I Tungsten, nickel, and copper powder characteristics

Powder	W	Ni	Cu
Vendor	OSRAM Sylvania	INCO	ACu Powder
Grade	M37	123	635
Purity	99.95 pct	99.8 pct	99.0 pct
Particle Size Distribution, μm			
D_{10}	3.9	4.8	8.5
D_{50}	12.1	11.2	13.1
D_{90}	32.1	26.2	17.4
Apparent Density, g/cm^3	3.5	3.1	4.2
Tap Density, g/cm^3	5.4	3.6	5.2
Pycnometer Density, g/cm^3	19.3	8.8	8.5
BET Surface Area, m^2/g	0.169	0.36	0.42

collected images were first transferred to binary files. Any artifact was removed by erosion and dilation functions and the resulting image was designated as A. Grain segregation was carried out to separate grain contact on A and this new image was designated as B. Then the A image was subtracted from the B image, giving a third image designated as C. Grain size and total interfacial area (grain boundary plus grain-liquid interface) were obtained from the B image. The grain boundary information was obtained from the C image. For each image, the frame edge-touching grains or grain boundaries were ignored in collecting data. More than 450 grains were analyzed for each sample.

4. Results

4.1. Density and porosity

Prior work [20] showed that an increase in the copper content increases compact swelling and reduces the temperature at which maximum swelling occurs. In these W-Ni-Cu systems, the copper effect on sample shape change is the opposite. The Ni : Cu = 8 : 2 samples show swelling and shape distortion while the Ni : Cu = 6 : 4 samples have no dimensional loss. Obviously, lack of solubility of tungsten in copper is beneficial for solid skeletal formation and preservation of compact shape during sintering, probably because nickel dissolves tungsten grain contacts and reduces the solid content and dihedral angle.

As shown in Table II, the samples had significant density changes during heating. Both compositions achieved a density over 95% after 1 min of microgravity sintering. For the Ni : Cu = 8 : 2 samples, the fractional density fluctuated around a mean of 0.933 while the Ni : Cu = 6 : 4 samples had a higher mean of 0.985. Since only one sample was available for each sintering time, no detailed trends were possible. We suspect that some of the density fluctuations were associated with pore agglomeration. For the Ni : Cu = 8 : 2 samples, there are large pores inside the samples; the sintered fractional density standard deviation is 0.015. For the Ni : Cu = 6 : 4 samples, there were no overall shape distortion or agglomerated large internal pores; the sintered fractional density standard deviation is 0.005.

Except the abnormally agglomerated pores in the Ni : Cu = 8 : 2 samples, the regular small pores in both the Ni : Cu = 8 : 2 and 6 : 4 samples were also analyzed. Due to the fewer number of pores in each sample, the whole cross section area was examined rather than using the sampling method as in grain size measurement. Table III gives the median pore size for the two Ni : Cu ratios and four sintering times. Even for these regular pores, it shows pore agglomeration with sintering. The smallest median pore size was for the 1 min sintered samples for both alloys. When the normalized pore size (the ratio of the actual pore size to the median pore size) cumulative frequency was plotted, different sintering time samples shown the same distribution pattern for both Ni : Cu ratios as shown in Figs 3 and 4.

TABLE III Median pore sizes of different Ni : Cu ratio samples after 1500°C microgravity sintering

Sintering Time (min)	Ni : Cu = 8 : 2 Pore Size (μm)	Ni : Cu = 6 : 4 Pore Size (μm)
1	5.88	5.95
45	6.86	8.16
180	14.34	12.73
600	10.57	9.11

4.2. Grain growth and contiguity

Grain growth is a dominant aspect of microstructural evolution during liquid phase sintering. In this study, the grain intercept size was obtained by the mean of the grain projections on 12 lines placed every 15° around a half circle, starting with the x-axis as 0° and going

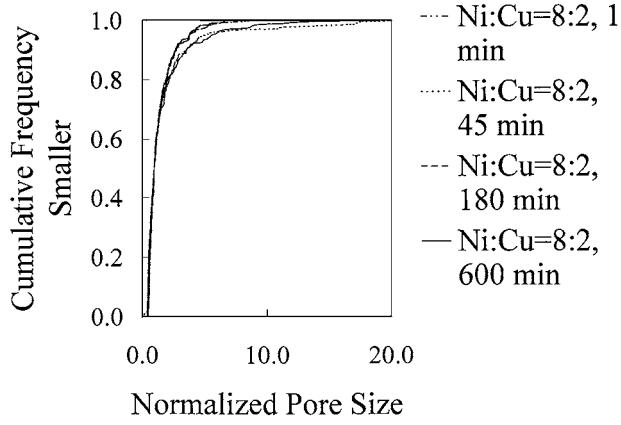

Figure 3 Plot of normalized pore size distribution for the Ni : Cu = 8 : 2 samples after microgravity sintering at 1500°C. The distribution pattern remains the same after different sintering times.

TABLE II Fractional densities before and after 1, 45, 180, and 600 min microgravity sintering at 1500°

Composition		88W(8 : 2)	88W(6 : 4)
Microscopic Observation	Overall Compact Cross Section	Swelling Pore Aggregation	No Distortion Uniformly Distributed Small Pores
Preflight Density		0.651 ± 0.010	0.645 ± 0.007
Sintered Density	1 min	0.952	0.983
	45 min	0.926	0.990
	180 min	0.935	0.977
	600 min	0.917	0.982
Mean Fractional Density		0.933	0.985
Fractional Density Standard Deviation		0.015	0.005

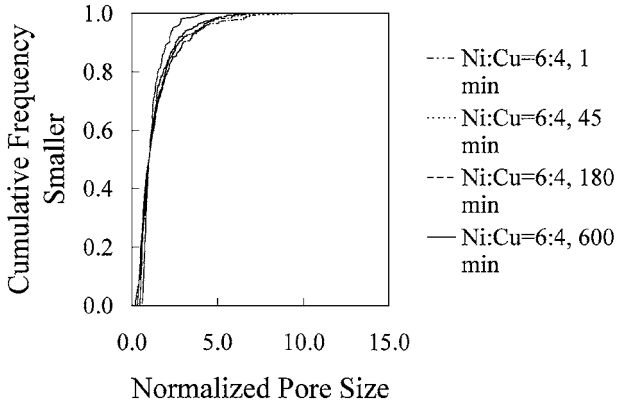

Figure 4 Plot of normalized pore size distribution for the Ni : Cu = 6 : 4 samples after microgravity sintering at 1500°C. The distribution pattern remains the same after different sintering times.

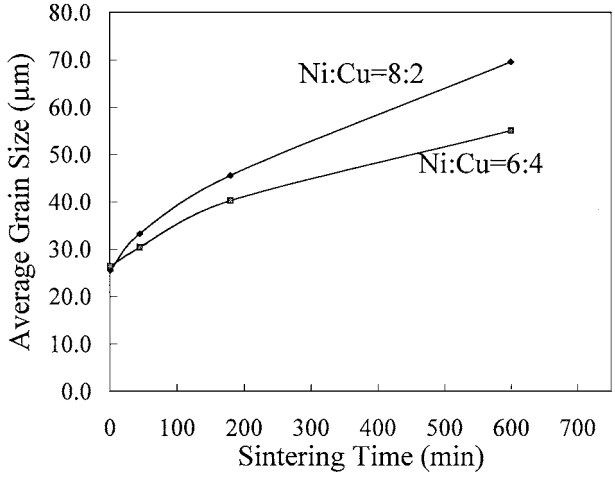

Figure 5 Grain size vs. sintering time for the 88W-Ni-Cu samples at 1500°C during microgravity sintering. The Ni : Cu = 6 : 4 samples always have smaller grain size than the Ni : Cu = 8 : 2 samples.

counterclockwise. Since the measured grain size was taken from a two-dimensional cross section, we multiplied $\frac{4}{\pi}$ to the original data to convert two-dimensional average intercept grain size to three-dimensional average grain size [11]. As shown in Fig. 5, the Ni : Cu = 8 : 2 and Ni : Cu = 6 : 4 samples have almost the same grain size after 1500°C, 1 min sintering. The grain size is twice the original tungsten particle size. As sintering continues, grain growth proceeds and grain sizes for both Ni : Cu ratio samples increase. The Ni : Cu = 6 : 4 samples always have smaller grains than the Ni : Cu = 8 : 2 samples. After 600 min sintering at 1500°C, the grain sizes for both compositions have doubled or tripled the 1 min sintering sample grain sizes.

The contiguity of the solid grains is a measure of the grain-grain contact area. As tabulated in Table IV, the mean contiguity for the Ni : Cu = 8 : 2 samples was 0.212, and for the Ni : Cu = 6 : 4 samples 0.269. The Ni : Cu = 6 : 4 samples always have a higher contiguity than the Ni : Cu = 8 : 2 samples. There are contiguity variations as sintering time increases.

4.3. Grain size distribution

Besides attention to grain growth during liquid phase sintering, there is concern with the evolution of a steady-state grain size distribution. Grain size distribution can be an effective indicator of coarsening process since the tendency for grains to grow or shrink depends on the grain size. In this study, a cumulative grain size distribution is generated and plotted in Figs 6 and 7 after different sintering times in microgravity at 1500°C. The grains size axis is on a logarithmic basis. For both the Ni : Cu = 8 : 2 and Ni : Cu = 6 : 4 samples, the grain sizes show the same distribution pattern where the grain size population locates around the median grain size. The shift of the distribution curves towards the larger grain sizes is an indication of continued grain growth with sintering time. If we examine the coefficient of variation for the grain size distribution (the ratio of the

TABLE IV Contiguity vs. sintering time at 1500°C in microgravity for the 88W-Ni-Cu (Ni : Cu = 8 : 2 and 6 : 4) samples

	Ni : Cu = 8 : 2		Ni : Cu = 6 : 4	
Sintering Time, min	Contiguity	Standard Deviation	Ni : Cu = 6 : 4 Contiguity	Standard Deviation
1	0.191	0.043	0.286	0.021
45	0.239	0.044	0.264	0.017
180	0.217	0.044	0.248	0.096
600	0.199	0.025	0.279	0.056
Mean Contiguity	0.212		0.269	
Contiguity Standard Deviation	0.021		0.017	

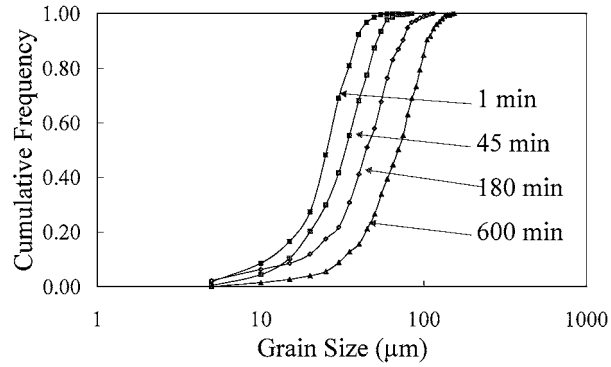

Figure 6 Cumulative grain size distribution vs. sintering time for the Ni : Cu = 8 : 2 samples at 1500°C in microgravity sintering. The distribution pattern remains the same after different sintering times.

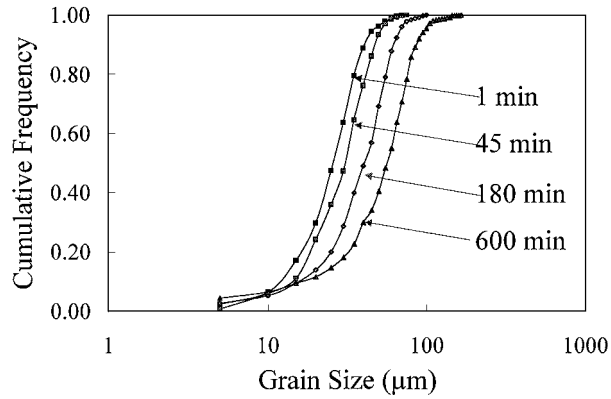

Figure 7 Cumulative grain size distribution vs. sintering time for the Ni : Cu = 6 : 4 samples at 1500°C in microgravity sintering. The distribution pattern remains the same after different sintering times.

standard deviation of grain size distribution to the median grain size) at different sintering times, it gives almost the same value for the same composition sample. The Ni : Cu = 8 : 2 samples have a value of 0.42 while the Ni : Cu = 6 : 4 samples have a value of 0.45.

5. Discussion

5.1. Macroscopic features

Previous studies have observed and reported stable pore structures in the microgravity sintered W-Ni-Fe samples [13, 14]. Combined with the current studies, our results substantiate previous suggestions of a buoyancy contribution to pore elimination during liquid phase sintering on Earth. When gravity is present, pores can be filled by the rearrangement of the solid skeleton or liquid motion through the solid skeleton. Under microgravity, such reorganization is not available without a long range driving force. Due to the lack of buoyancy force, large pores cannot escape from the sample, remaining in equilibrium with the solid and liquid phases, and allowing pore coalescence to reduce the system energy [12].

Lack of buoyancy in microgravity successfully explained the persistence of pores and their enlargement through agglomeration. For the Ni : Cu = 8 : 2 and Ni : Cu = 6 : 4 samples, the solid solubility in the liquid phase differs; the higher dihedral angle of the Ni : Cu = 8 : 2 samples gives anomalous pore morphologies since they have been processed under the same conditions and had the same density before flight. When the nickel content is high (Ni : Cu = 8 : 2), newly formed liquid dissolves solid tungsten more easily; the smaller dihedral angle from this composition allows the liquid to penetrates between the grains. This breaks up the solid skeleton and coats the grain with liquid. Under the surface tension of the liquid, solid grains rearrange. This causes structural reorganization, liquid redistribution, and possibly pore coalescence. When the new skeleton is formed quickly at such high sintering temperature, liquid filling of pores is not efficient enough to eliminate porosity. Once the solid skeleton reforms, the entrapped pores remain stable. This causes compact swelling and distortion. When the nickel content is low (Ni : Cu = 6 : 4), the solubility of solid tungsten in the liquid decreases. The stable solid skeleton in newly formed liquid sustains compact rigidity. The sample shape is retained with no swelling and distortion. Under capillary pressure, pore filling proceeds and the structure remains stable up to nearly full densification.

5.2. Grain growth

Different Ni : Cu ratios show no significant effect on grain growth during the initial stage of sintering. The average grain sizes for both compositions are the same after 1 min sintering at 1500°C. Note the median tungsten particle size (based on mass) was 12.1 μm before sintering and the median grain size (based on population) was 26 μm after 1 min sintering at 1500°. Since population median size is always smaller than mass median size, it is clear that grain size has at least doubled during this initial sintering for both compositions.

In the presence of the liquid phase, solution-reprecipitation proceeds by the dissolution and reprecipitation of smaller tungsten grains on to the larger tungsten grains. When the liquid has high solubility for the grains, tungsten concentration in the liquid phase increases. According to the analysis in Section 2, the coarsening rate through the liquid phase increases. Coalescence takes place by the fusion of grains that are in contact with each other. As sintering continues, grain-grain contact increases; grain coarsening through solid diffusion also increases according to Equation 19. The importance of any one process on grain growth depends on the composition and processing conditions.

For the 88W-Ni-Cu systems, due to the rapid elimination of porosity in the initial appearance of the liquid phase, we can temporarily ignore porosity effects on grain growth and only consider liquid and solid diffusion events. With the simultaneous multiple phase diffusion, the operative mechanisms which influence the grain growth at any time can be analyzed from Equation 24. We can start the analysis with solid diffusion. When the solid grains are in contact, the neck size ratio between two contacting grains depends on the dihedral angle, which is a function of the system thermodynamics ($\frac{\gamma_{SS}}{\gamma_{SL}}$) [21]. Since nickel has high solubility of tungsten, the Ni : Cu = 8 : 2 sample has small γ_{SL} and consequently low dihedral angle from Equation 25. As expressed in Equation 26, the smaller the dihedral angle ϕ, the smaller the equilibrium neck size ratio. Contiguity, as a measure of neck size ratio, fits this analysis well as shown in Table IV (contiguity data in three dimensions are the same as measured in two dimensions [22]). If we substitute the contiguity values in Table IV and the grain size data in Fig. 5 into Equation 24, the grain growth rate constants can be calculated and the results are shown in Fig. 8.

$$\frac{\gamma_{SS}}{\gamma_{SL}} = 2\cos\left(\frac{\phi}{2}\right) \tag{25}$$

$$\frac{X}{G} = \sin\left(\frac{\phi}{2}\right) \tag{26}$$

X: neck diameter.

From Fig. 8, it is clear that the liquid diffusion grain growth rate constant K_L is the major contributor to grain growth. K_L is at least one order of magnitude larger than the solid diffusion grain growth rate constant K_S for both Ni : Cu ratios. An increase in copper content by 20% in the matrix decreases K_L by 46%. This is in accord with the tungsten solubility in nickel and copper. When the copper content is high, tungsten concentration in the liquid matrix decreases. As shown in Equation 21, this induces a lower K_L and decreases the overall grain growth rate constant K. Judging from Equations 2, 3, and 4, this results in smaller grain sizes for the higher copper content system (Fig. 5).

The Ni : Cu ratio also has an obvious effect on contiguity. The higher the copper content, the higher the contiguity. This agrees with the theoretical expectations from Equations 25 and 26. As sintering time increases, there is some contiguity fluctuation. German [23] attributed this to the transients of the grain boundary or

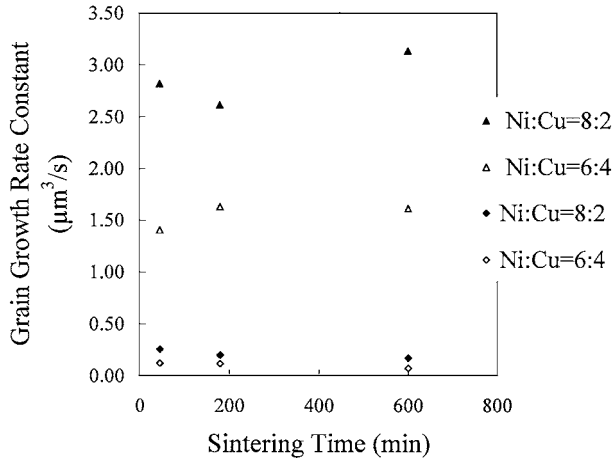

Figure 8 Calculated liquid diffusion grain growth rate constant K_L and solid diffusion grain growth rate constant K_S at different Ni : Cu ratios for the samples sintered at 1500°C in micorgravity. Higher copper content reduces the liquid diffusion grain growth rate constant K_L; the solid diffusion grain growth rate constant K_S is about one order of magnitude smaller than the liquid diffusion grain growth rate constant K_L. The triangle symbols are for the liquid diffusion grain growth rate constant K_L and the diamond symbols are for the solid diffusion grain growth rate constant K_S.

the solid-liquid surface energy (γ_{SS} and γ_{SL}). Since the surface energy varies during the initial portion of liquid phase sintering, a corresponding contiguity variation occurs. After the reorganization of stable and unstable grain contacts, final contiguity is decided by the interfacial energy between different phases.

When the copper content is high, the solubility of tungsten in the liquid phase decreases. This means that liquid volume fraction V_L and equilibrium tungsten concentration in the liquid C_{LO} decrease. German [4, 23] isolated liquid volume fraction effect on the overall grain growth rate constant in liquid phase sintering and summarized the following form :

$$K = K_I + \frac{K_{slope}}{V_L^{2/3}} \tag{27}$$

where K_I is an intercept value and K_{slope} is the slope of the grain growth rate constant variation with the liquid volume fraction V_L. Using the overall grain growth rate constant K derived from the current experimental data and assuming tungsten solubility varies linearly with Ni : Cu ratio, K_I and K_{slope} can be obtained as 61.38 and -23.78 $\mu m^3/s$ respectively for the 88W-Ni-Cu system. From Equations 21 and 27, the overall grain growth rate constant decreases as copper content increases.

From the above K_I and K_{slope} values, we can calculate the overall grain growth rate constant K variation solely due to liquid volume fraction change induced by different Ni : Cu ratios. The results are shown in Fig. 9 using initial liquid phase fraction as x-axis. For the same liquid content, the Ni : Cu = 8 : 2 samples always have a higher overall grain growth rate constant compared to the Ni : Cu = 6 : 4 samples.

When porosity exists in the system, the corresponding effect on grain growth depends on the location of pores in the sample. If pores are in the liquid matrix and separated from the grains, the porosity effect is

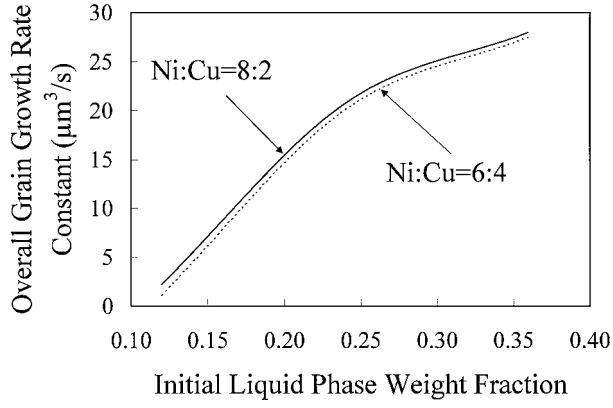

Figure 9 Calculated change in overall grain growth rate constant K due to Ni : Cu ratio effect on liquid content. X-axis is the initial liquid phase fraction. The results indicate that copper content increase reduces the overall grain growth rate constant K by reducing liquid volume fraction.

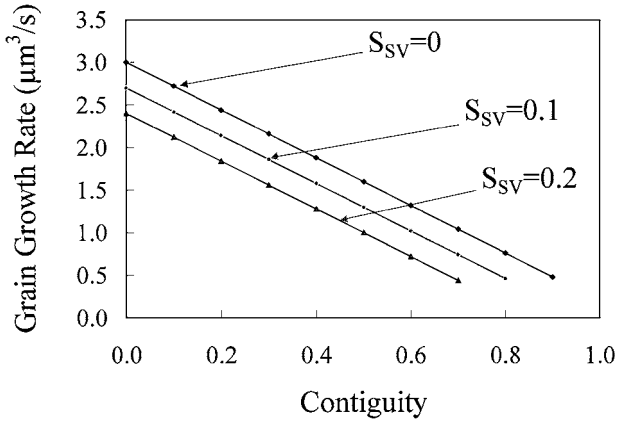

Figure 10 Prediction of pore-grain interfacial area effect on the grain growth rate constant K during sintering. S_{SV} represents the fractional pore-solid interfacial area around a grain. It shows that when the pores are attached to the grain and increase pore-grain interfacial area, the overall grain growth rate constant K decreases. The larger the pore-grain interfacial area, the smaller the grain growth rate constant K.

negligible since these isolated pores have no obvious effect on the controlling diffusion path. If pores are attached to the grains, they will reduce the solid-liquid and grain boundary areas and consequently affect the grain growth rate. Suppose the contiguity of the system (grain boundary area) is fixed and pores only reduce solid-liquid interfacial area, pores will reduce the overall grain growth rate constant K as shown in Fig. 10 for the Ni : Cu = 8 : 2 system. As contiguity increases, the overall grain growth rate constant K of different pore-grain interfacial area sample decreases at the same degree. At the same contiguity, the overall grain growth rate constant K decreases when pore-grain interfacial area increases. This calculation is carried out based on the assumption that pore reduces grain-liquid interfacial area by different fraction of total grain surface area as indicated in Fig. 10. From this assumption, it is clear that porosity effect on grain growth is decided by how much grain surface area is in contact with pores rather than by the pore size or the pore volume in the sample. Since pore attachment to the grain depends on the composition properties and probably processing parameters, it is difficult to draw the connection between

pore content and pore location in the sample from this study. This problem, however, can be an interesting topic for future study.

5.3. Grain size distribution

Grain size distribution is determined by a host of factors during sintering. Over the years, much effort has gone into quantification of grain size distribution in microstructure formed by liquid-phase sintering [24–27]. Experiments and computer simulations [25, 26] showed emergence of the self-similar distribution with widely varying initial particle size distributions. Wakai *et al*. [27] modeled the process of boundary motion through minimization of the boundary energy. Similar to German and Olevsky [4] and Fang and Patterson [25, 26], they showed that the grain size distribution normalized by the mean grain size converged during normal grain growth. Based on liquid phase sintering grain size distribution data [4], the cumulative intercept grain size distribution $F(G)$ can be described by :

$$F = 1 - \exp\left[-a\left(\frac{G}{G_{\mathrm{M}}}\right)^{n}\right] \tag{28}$$

a and n are constants; G_{M} is median grain size.

In this study, we started with log-normal particle size distribution powders and examined the grain size distribution curves at 1500°C following different sintering times. To avoid any bias in the assumed distribution, the normalized grain size (the ratio of the actual grain size G to the median grain size G_{M}) was utilized in the examination. Figs 11 and 12 show that for both Ni : Cu ratio samples, the normalized grain size distribution retains a self-similar pattern. Normalized grain size distribution reflects a grain size scattering around the median grain size as sintering time increases. After 1500°C, 1 min microgravity sintering, the grain size distribution has the highest frequency peak around 1.1 times the normalized grain size. As sintering time increases, the distribution frequency peak decreases. After 1500°C, 600 min microgravity sintering, the distribution has the lowest frequency peak around 1.1 times the normalized grain size.

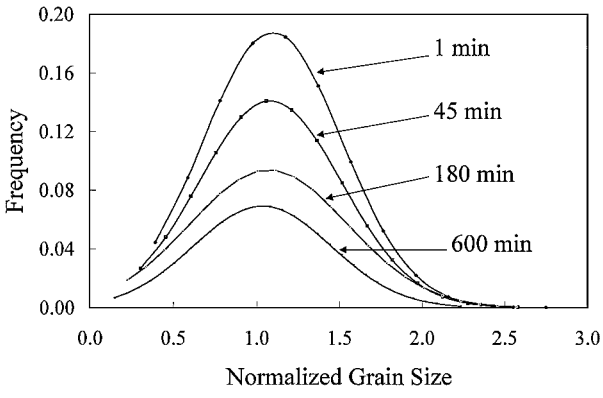

Figure 11 Plot of normalized grain size distribution for the Ni : Cu = 8 : 2 samples after microgravity sintering at 1500°C. The curves are obtained after fitting the experimental data. Normalized grain size is the ratio of the measured grain size to the median value of the measurement values.

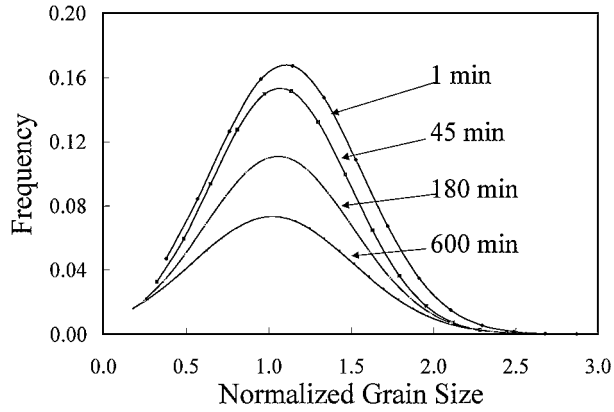

Figure 12 Plot of normalized grain size distribution for the Ni : Cu = 6 : 4 samples after microgravity sintering at 1500°C. The curves are obtained after fitting the experimental data. Normalized grain size is the ratio of the measured grain size to the median value of the measurement values.

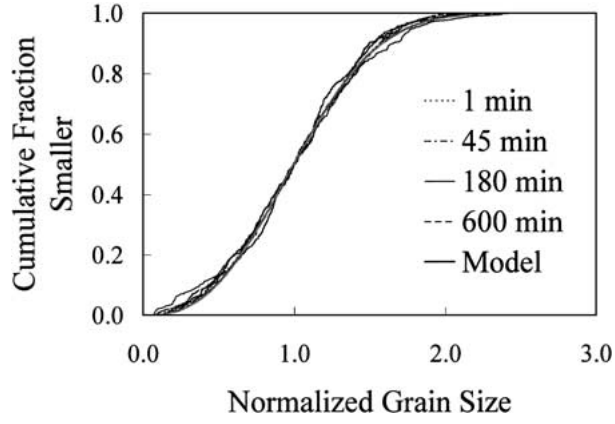

Figure 13 Normalized grain size distribution for the Ni : Cu = 8 : 2 samples showing the self-similar pattern at different sintering times. The model curve is obtained by Equation 27 with a and n values of 0.7 and 2.6.

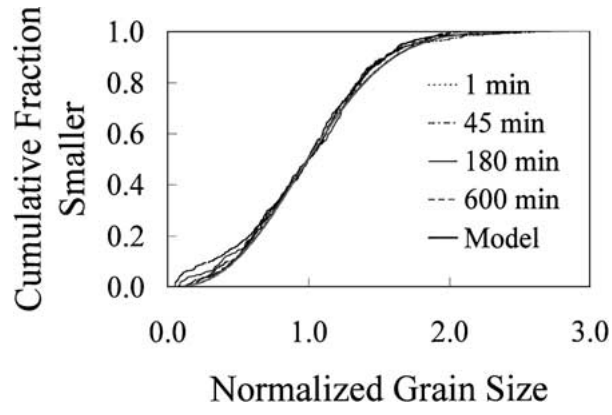

Figure 14 Normalized grain size distribution for the Ni : Cu = 6 : 4 samples showing the self-similar pattern at different sintering times. The model curve is obtained by Equation 27 with a and n values of 0.7 and 2.6.

If we plot the normalized grain size distribution at different Ni : Cu ratios as shown in Figs 13 and 14, the normalized grain sizes fall on the same distribution curve. From the curve, we can extract a and n values in Equation 28 and compare with the previous proposed values. In this experiment, n equals 2.6 while a is 0.7 for both the Ni : Cu = 8 : 2 and the Ni : Cu = 6 : 4 samples.

For the same a value, n value in this study is larger than the proposed value of 2 in the previous model [4]. Further studies are desirable for the explanation of this discrepancy of microgravity results.

6. Conclusions

In liquid phase sintering, the liquid provides an important diffusion path for grain coarsening while the grain-grain contacts provide a diffusion route for grain coalescence. In the absence of residual pores, solid grain contact is determined by the solid content and solid-liquid interfacial energy. For many systems, solid diffusion across contact grain boundaries is an important contribution to grain growth. In this study, multiple diffusion events were analyzed utilizing microgravity sintered samples. Copper content has a pivotal role in determining sample distortion. As the copper content increases in the W-Ni-Cu system, the increase in solid phase contiguity favors the formation of a rigid skeleton. Through calculation, it shows that liquid diffusion grain growth rate constant K_L is at least one order of magnitude larger than solid diffusion grain growth rate constant K_S. Copper increase also suppresses the overall grain growth rate constant K, mainly by decreasing liquid diffusion grain growth rate constant K_L. Relative grain size distributions remain self-similar regardless of composition and sintering time. The experimental data fit a common equation even though the extracted constant n deviates from the model proposed before.

Acknowledgments

Research funding on the gravitational role in liquid phase sintering was provided by NASA. We would also like to thank Lou Campbell for providing generous help in the microstructural measurements and Anish Upadhyaya for preparing the samples.

References

1. R. GANESAN, A. GRIFFO and R. M. GERMAN, *Metall. Mater. Trans.* **29A** (1998) 659.
2. I. M. LIFSHITZ and V. V. SLYZONOV, *J. Phys. Chem. Solids* **19** (1961) 35.
3. C. WAGNER, *Z. Elektrochem* **65** (1961) 581.
4. R. M. GERMAN and E. A. OLEVSKY, *Metall. Mater. Trans.* **29A** (1998) 3057.
5. Y. LIU, D. F. HEANEY and R. M. GERMAN, *Acta Metall. Mater.* **43** (1995) 1587.
6. R. M. GERMAN, Y. LIU and A. GRIFFO, *Metall. Mater. Trans.* **28A** (1997) 215.
7. R. M. GERMAN, *ibid.* **26B** (1995) 649.
8. J. L. JOHNSON, A. UPADHYAYA and R. M. GERMAN, *ibid.* **29B** (1998) 857.
9. S. KOHARA and M. HOSHINO, in "Advances in Powder Metallurgy and Particulate Materials" (Metal Powder Industries Federation, Princeton, New Jersey, 1994) p. 295.
10. S. KOHARA and T. OHIRA, in Proceedings of Powder Metallurgy World Congress, Kyoto, 1993, edited by Y. Bando and K. Kosuge (Japan Society of Powder and Powder Metallurgy, 1993) p. 909.
11. I. SEYHAN, L. RATKE, W. BENDER and P. W. VOORHEES, *Metall. Mater. Trans.* **27A** (1996) 2470.
12. Y. LIU, R. G. IACOCCA, J. L. JOHNSON, R. M. GERMAN and S. KOHARA, *ibid.* **26A** (1995) 2484.
13. R. M. GERMAN, R. G. IACOCCA, J. L. JOHNSON, Y. LIU and A. UPADHYAYA, *JOM-J. Min. Met. Mat.* **S47** (1995) 46.
14. J. NASER, J. E. SMITH JR and A. K. KURUVILLA, *J. Mater. Sci.* **33** (1998) 5573.
15. E. A. OLEVSKY and R. M. GERMAN, *Acta Mater.* **48** (2000) 1153.
16. E. A. OLEVSKY, R. M. GERMAN and A. UPADHYAYA, *ibid.* **48** (2000) 1167.
17. J. E. BURKE and D. TURNBULL, *Prog. Metall. Phys.* **3** (1952) 220.
18. M. HILLERT, *Acta Metall.* **13** (1965) 227.
19. G. W. GREENWOOD, *ibid.* **4** (1956) 243.
20. A. UPADHYAYA and R. M. GERMAN, *Int. J. Powder Metall.* **34** (1998) 43.
21. R. M. GERMAN, *Metall. Trans.* **16A** (1985) 1247.
22. E. E. UNDERWOOD, in "Quantitative Stereology" (Addison-Wesley, Reading, MA, 1970) p. 109.
23. R. M. GERMAN, in "Sintering Theory and Practice" (John Wiley & Sons, New York, 1996) p. 225.
24. S.-C. YANG and R. M. GERMAN, *Scripta Metallugrica et Materialia* **26** (1991) 95.
25. Z. FANG, B. R. PATTERSON and M. E. TURNER, *Acta Metall. Mater.* **40** (1992) 713.
26. *Idem., Mater. Characterization* **31** (1993) 177.
27. F. WAKAI, N. ENOMOTO and H. OGAWA, *Acta Mater.* **48** (2000) 1297.

Received 5 July
and accepted 28 November 2000